Inorg. Chem. **2007**, *46*, 10079–10086

Magnetic Properties and Magnetic Structures of $Cu_3(OD)_4XO_4$, X = Se or S: Cycloidal versus Collinear Antiferromagnetic Structure

Serge Vilminot,*,† Gilles André,‡ Francoise Bourée-Vigneron,‡ Mireille Richard-Plouet,§ and Mohamedally Kurmoo*,||

Groupe des Matériaux Inorganiques, IPCMS, UMR 7504 CNRS-ULP, 23 rue du Loess, BP 43, 67034 Strasbourg Cedex 2, France, Laboratoire Léon Brillouin, CEA-CNRS, CEA-Saclay, 91191 Gif-sur-Yvette Cedex, France, Institut des Matériaux Jean Rouxel, UMR CNRS 6502, Université de Nantes, 2 rue de la Houssinière, BP 32229, 44322 Nantes Cedex 03, France, and Laboratoire de Chimie de Coordination Organique, CNRS-UMR7140, Université Louis Pasteur, Institut Le Bel, 4 rue Blaise Pascal, 67000 Strasbourg Cedex 01, France

Received May 9, 2007

We report a comparative study of the magnetic properties of synthetic $Cu_3(OH)_4(SO_4)_x(SeO_4)_{1-x}$ and the magnetic structures of the parent compounds. All compounds are isostructural and belong to the orthorhombic class of parent compounds. They consist of 3-legged ribbons of edge-sharing copper octahedra connected by μ_3-OH and XO_4 (X = S or Se). XO_4 acts both as one-atom and three-atom bridges to connect seven Cu atoms (six Cu(2) and one Cu(1)) belonging to three neighboring ribbons. The two end members behave as low-dimensional AF with a long-range antiferromagnetic state below 5 (X = S) and 8 K (X = Se); the former shows evidence of a canting. Analyses of the neutron powder diffraction data for X = S were shown to display an ordered magnetic state (k = 0 0 0) where the moments of Cu(2) within the two outer legs are collinear and parallel within each leg but antiparallel from each other; the orientation of the moments of Cu(2) is the c axis. In contrast, for X = Se $k = \sim 1/7\ 0\ 0$ and the magnetic structure is cycloidal and transforms progressively from being incommensurate ($T > 3$ K) to commensurate ($T \leq 3$ K). The moments of Cu(2) of each leg are oriented antiparallel as for X = S, but they rotate about the b axis while propagating along the a axis. In both cases the moments of Cu(1) of the inner leg remain random. The magnetic entropy of 15.2 ± 1 J/kmol for the end members, estimated from integrating the heat capacity/temperature, is close to that expected ($3R$ ln 2) for three Cu^{2+} (S = 1/2).

Introduction

Considerable efforts are being made to create and understand the behavior of new magnetic materials in view of the large-scale industrial application for information storage.[1] To date these efforts are divided into different key areas, such as pure and alloyed metals, metal oxides, and metal−organic hybrids.[2−4] On a less active side, several groups are interested in existing magnetic minerals and especially in reproducing them in pure forms in the laboratory.[5] To this end, we and others have recently studied several hydroxy sulfates of the transition metals Mn, Co, Ni, and Cu.[6,7] Our original interests were several fold: (a) to find optimized conditions to synthesize these materials in high purity and large quantities

* To whom correspondence should be addressed. S.V.: Phone, 00 33 3 88 10 71 28; Fax, 00 33 3 88 10 72 47; E-mail, vilminot@ipcms.u-strasbg.fr. M.K.: Phone, 00 33 3 90 24 13 56; Fax, 00 33 3 90 24 13 25; E-mail, kurmoo@chimie.u-strasbg.fr.

† IPCMS, Strasbourg.

‡ Laboratoire Léon Brillouin, Gif-sur-Yvette.

§ Université de Nantes.

|| Université Louis Pasteur, Strasbourg.

(1) See Proceedings of the International Conference on Magnetism. *J. Mag. Mag. Mater.* **2007**, *310* (2).

(2) See (a) Proceedings of the International Symposium on Physics of Magnetic Materials. *J. Mag. Mag. Mater.* **2006**, *303* (2). (b) Proceedings of the International Symposium on Spintronics and Advanced Magnetic Technologies and International Symposium on Magnetic Materials and Applications 2005. *J. Mag. Mag. Mater.* **2006**, *304* (1).

(3) See Proceedings of the International Symposium on Soft Magnetic Materials. *J. Mag. Mag. Mater.* **2006**, *304* (2).

(4) See Proceedings of the International Conference on Molecule-based Magnets (ICMM). *Polyhedron* **2003**, *22* (14−17). See Proceedings of the International Conference on Molecule-based Magnets (ICMM). *Polyhedron* **2005**, *24* (16−17).

(5) *Handbook of Hydrothermal Technology, Technology for Crystal Growth and Material Processing*; Byrappa, K., Yoshimura, M., Eds.; William Andrew Publishing: New York, 2001.

10.1021/ic700900b CCC: $37.00
Published on Web 10/31/2007

as well as synthesizing their deuterated forms, (b) to study their magnetic properties and heat capacities as a function of temperature and field, and (c) to determine their magnetic structures from their neutron powder diffraction. In addition to succeeding in obtaining known minerals, several new phases were also obtained and studied. In the process several unusual properties were encountered, for example, (a) the coexistence of short- and long-range magnetic ordering and (b) observation of an idle moment in the ordered magnetic state.[6] The latter was observed for $Cu_3(OH)_4SO_4$, known as Antlerite in the natural form. To explore this particular property we studied the selenate analogue and here present the results of this work. Although it is isostructural to $Cu_3(OH)_4SO_4$, its magnetic properties and, in particular, magnetic structure are quite different. While $Cu_3(OH)_4SO_4$ was found to exhibit clear evidence of a canted-antiferromagnetic state below 5 K and an almost collinear magnetic structure, $Cu_3(OH)_4SeO_4$ displays a compensated Néel state below 8 K but has, in contrast to $Cu_3(OH)_4SO_4$, a cycloidal magnetic structure which is incommensurate above 3 K and becomes progressively commensurate at and below 3 K. In addition, we present the results of the magnetic properties of three solid solutions of SO_4/SeO_4.

Cycloidal and/or incommensurate magnetic structures are rarely observed for molecular and mineral systems. Incommensurate magnetic structures are more frequently encountered in ternary intermetallic compounds containing rare-earth elements, and very few examples have been evidenced for 3d transition metals. An incommensurate magnetic structure consists of a modulation of either the magnetic moment with constant orientation (sinusoidal model) or the orientation with constant magnetic moment (e.g., spiral, helicoidal, or cycloidal model).[8] For the spiral model, the magnetic moments rotate outside a plane comprising the propagation vector, whereas for the cycloidal model they rotate inside this plane. Moreover, the incommensurate structure is not always observed for all temperatures below T_C or T_N. In several cases, the incommensurability locks with the lattice at a temperature below the long-range magnetic transition. The propagation vector that describes the modulation direction and rotation angle can be constant or not. More complicated models have also been evidenced but will not be referred here. A few examples will be summarized to illustrate the above considerations.

For ternary compounds, a spiral structure has been evidenced for berthierite $FeSb_2S_4$ with a constant propagation vector $k = (0.394, 0, 0)$ for all temperatures between 5 K and $T_N = 50$ K.[9] A constant propagation vector is also observed between 1.5 K and $T_N = 42$ K for $Cr_{0.5}TiSe_2$ with $k = (0.0386, 0, 0.4229)$ with a spiral model.[10] In $TlCo_2Se_2$, the propagation vector slightly decreases with increasing temperature.[11] For the compounds Er_6TX_2 (T = Mn, Fe, Co and X = Sb, Bi) having the Zr_6CoAs_2-type structure, an incommensurate spiral magnetic structure is evidenced only for Er_6MnBi_2 with a constant propagation vector $k = (0.596, 0, 0)$ for $2\text{ K} < T < 33$ K, well below $T_C = 100$ K.[12] It has to be mentioned that magnetic order, commensurate or incommensurate, is only achieved for the rare earth whatever the 3d and X elements. Cycloidal magnetic structures have been observed for $DyFe_4Al_8$ and $HoFe_4Al_8$[13] with ordering of the Fe sublattice first, the rare-earth ordering taking place at lower temperature and following the modulation of the Fe sublattice. Other examples are given by $GdCu_2$ with a commensurate cycloidal model ($k = 2/3, 1, 0$)[14] and IrMnSi with an incommensurate cycloidal magnetic structure with a 3.8 μ_B moment on Mn atoms;[15] no magnetic moment was detected on Ir atoms, and the k_z component of the propagation vector (0, 0, k_z) increases very slightly with increasing temperature.

For metal oxides, the manganese oxides exhibit peculiar magnetic structures with an incommensurate spiral model for β-MnO_2 (pyrolusite),[16] a commensurate−incommensurate magnetic transition at 33 K for Mn_3O_4 ($T_C = 42$ K),[17] and a complex magnetic ordering for α-Mn_2O_3.[18] A commensurate ($10\text{ K} < T < T_N = 21$ K)−incommensurate ($T < 10$ K) transition has also been evidenced in CuB_2O_4.[19] A similar transition is observed in VPO_4, but the incommensurate spiral magnetic structure appears at $10.3 < T < T_N = 25.5$ K,[20]

(6) (a) Vilminot, S.; Richard-Plouet, M.; André, G.; Swierczynski, D.; Bourée-Vigneron, F.; Marino, E.; Guillot, M. *Cryst. Eng.* **2002**, *5*, 177. (b) Vilminot, S.; Richard-Plouet, M.; André, G.; Swierczynski, D.; Guillot, M.; Bourée-Vigneron, F.; Drillon, M. *J. Solid State Chem.* **2003**, *170*, 255. (c) Vilminot, S.; Richard-Plouet, M.; André, G.; Swierczynski, D.; Bourée-Vigneron, F.; Kurmoo, M. *Dalton Trans.* **2006**, 1455−1462. (d) Ben Salah, M.; Vilminot, S.; André, G.; Richard-Plouet, M.; Bourée-Vigneron, F.; Mhiri, T.; Kurmoo, M. *Chem. Eur. J.* **2004**, *10*, 2048. (e) Ben Salah, M.; Vilminot, S.; Mhiri, T.; Kurmoo, M. *Eur. J. Inorg. Chem.* **2004**, 2272. (f) Vilminot, S.; Richard-Plouet, M.; André, G.; Swierczynski, D.; Bourée-Vigneron, F.; Kurmoo, M. *Inorg. Chem.* **2003**, *42*, 6859. (g) Ben, Salah, M.; Vilminot, S.; André, G.; Richard-Plouet, M.; Mhiri, T.; Takagi, S.; Kurmoo, M. *Chem. Mater.* **2005**, *17*, 2612. (h) Ben Salah, M.; Vilminot, S.; André, G.; Richard-Plouet, M.; Bourée-Vigneron, F.; Mhiri, T.; Kurmoo, M. *J. Am. Chem. Soc.* **2006**, *128*, 7972.

(7) (a) Nocera, D. G.; Bartlett, B. M.; Grohol, D.; Papoutsakis, D.; Shores, M. P. *Chem. Eur. J.* **2004**, *10*, 3850 and references therein. (b) Wills, A. S. *Phys. Rev. B.* **2001**, *63*, 064430. (c) Shores, M. P.; Nytko, E. A.; Bartlett, B. M.; Nocera, D. G. *J. Am. Chem. Soc.* **2005**, *127*, 13462. (d) Harrison, A. *J. Phys: Condens. Matter.* **2004**, *16*, S553. (e) Behara, J. N.; Rao, C. N. R. *Can. J. Chem.* **2005**, *83*, 668−673. (f) Behara, J. N.; Rao, C. N. R. *Dalton Trans.* **2007**, 668−673.

(8) http://www.answers.com/topic/cycloid: A cycloid is the curve defined by a fixed point on a wheel as it rolls or, more precisely, the locus of a point on the rim of a circle rolling along a straight line.

(9) Wintenberger, M.; André, G. *Physica B* **1990**, *162*, 5−12.

(10) Baranov, N. V.; Titov, A. N.; Maksimov, V. I.; Toporova, N. V.; Daoud-Aladine, A.; Podlesnyak, A. *J. Phys. Condens. Matter* **2005**, *17*, 5255−5262.

(11) Lizarraga, R.; Ronneteg, S.; Berger, R.; Bergman, A.; Mohn, P.; Eriksson, O.; Nordström, L. *Phys. Rev. B* **2004**, *70*, 024407−1−7.

(12) Morozkin, A. V.; Nirmala, R.; Malik, S. K. *J. Alloys Compd.* **2005**, *394*, 75−79.

(13) Paixao, J. A.; Ramos Silva, M.; Sorensen, S. Aa.; Lebech, B.; Lander, G. H.; Brown, P. J.; Langridge, S.; Talik, E.; Gonçalves, A. P. *Phys. Rev. B* **2000**, *61*, 6176−6188.

(14) Rotter, M.; Lindbaum, A.; Gratz, E.; Hilscher, G.; Sassik, H.; Fischer, H. E.; Fernandez-Diaz, M. T.; Arons, R.; Seidl, E. *J. Magn. Magn. Mater.* **2000**, *214*, 281−290.

(15) Eriksson, T.; Bergqvist, L.; Burkert, T.; Felton, S.; Tellgren, R.; Nordblad, P.; Eriksson, O.; Andersson, Y. *Phys. Rev. B* **2005**, *71*, 174420−1−10.

(16) (a) Yoshimori, A. *J. Phys. Soc. Jpn.* **1959**, *14*, 807. (b) Regulski, M.; Przenioslo, R.; Sosnowska, I.; Hoffmann, J.-U. *Phys. Rev. B* **2003**, *68*, 172401−1−4.

(17) Chardon, B.; Vigneron, F. *J. Magn. Magn. Mater.* **1986**, *58*, 128.

(18) (a) Przenioslo, R.; Regulski, M.; Sosnowska, I.; Hohlwein, D. *BENSC Exp. Rep.* **1999**, *1998*, 41. (b) Reguslski, M.; Przenioslo, R.; Sosnowska, I.; Hohlwein, D.; Schneider, R. *J. Alloys Compd.* **2004**, *362*, 236.

Table 1. Results of the Elemental Analyses[a] of the Mixed S/Se Samples

starting S:Se	EDX	XRPD	ICP	final composition
3:1	$(SO_4)_{0.61}(SeO_4)_{0.39}$	$(SO_4)_{0.59}(SeO_4)_{0.41}$		$Cu_3(OH)_4(SO_4)_{0.60}(SeO_4)_{0.40}$
1:1	$(SO_4)_{0.32}(SeO_4)_{0.68}$	$(SO_4)_{0.31}(SeO_4)_{0.69}$	$(SO_4)_{0.28}(SeO_4)_{0.72}$	$Cu_3(OH)_4(SO_4)_{0.30}(SeO_4)_{0.70}$
1:3	$(SO_4)_{0.08}(SeO_4)_{0.92}$	$(SO_4)_{0.10}(SeO_4)_{0.90}$	$(SO_4)_{0.09}(SeO_4)_{0.91}$	$Cu_3(OH)_4(SO_4)_{0.09}(SeO_4)_{0.91}$

[a] The EDX of the end members gives a Cu:Se or S ratio of 3:1.

the propagation vector $k = (k_x, 0, 0)$ increasing with increasing temperature from 0.5 to 0.561, the magnetic structure being commensurate for $T \leq 10.3$ K with $k_x = 0.5$. In the $M^{II}As_2O_6$ family, M = Mn, Co, and Ni, an incommensurate spiral magnetic structure is evidenced only for Mn.[21] Finally, we can mention the case of the multiferroic compound $BiFeO_3$ with a distorted cycloidal magnetic modulation with a propagation vector $k = (0.0045, 0.0045, 0)$;[22] the model remains the same from 4 K up to $T_N = 640$ K. These few examples illustrate the richness and, in some cases, complexity of the spiral and cycloidal magnetic structures; this information may be interesting, at this modest level, for readers who are not familiar with the field.

Experimental Section

Synthesis. Copper selenate pentahydrate was first prepared by reaction of copper oxide, CuO (2.26 g, Prolabo, 99%), and selenic acid, H_2SeO_4 (10.38 g, Aldrich, 99.95%, 40 wt % solution), in aqueous solution. After evaporation of water, $CuSeO_4 \cdot 5H_2O$ crystallizes as big blue crystals that were identified by X-ray powder diffraction (JCPDF file No. 20-363). $Cu_3(OH)_4SeO_4$ was prepared by hydrothermal treatment of a suspension obtained from $CuSeO_4 \cdot 5H_2O$ (2.21 g) and NaOH (0.398 g, Prolabo, 98%) in 15 mL of water having a molar ratio of 3:4:333. The hydrothermal reaction was performed under autogenous pressure in Teflon-lined autoclaves of 125 mL at 240 °C for 72 h. The autoclaves were then quenched in cold water, and the solid products were separated from the clear mother liquor by filtration, washed several times with distilled water to remove soluble salts and then with ethanol and acetone, and finally dried in air. $Cu_3(OH)_4SeO_4$ was obtained as a green powder in almost quantitative yield. Samples for neutron powder diffraction, containing over 90% of OD, were prepared in a similar manner by replacing normal water by heavy water. $Cu_3(OH)_4SO_4$ and $Cu_3(OD)_4SO_4$ were reported previously.

Mixed sulfate/selenate samples were prepared by the hydrothermal treatment of suspensions obtained from $CuSO_4 \cdot 5H_2O$, $CuSeO_4 \cdot 5H_2O$, and NaOH with respective proportions S/Se of 3, 1, and 0.333, all other conditions being similar to the preparation of the pure selenate, i.e., (S + Se)/NaOH/H_2O molar ratio of 3:4:333 and reaction performed under autogenous pressure at 240 °C for 72 h. The products were then washed with water, alcohol, and acetone and finally dried in air. The first observation is that the resulting powders have a significantly lighter green color than $Cu_3(OH)_4SO_4$ and $Cu_3(OH)_4SeO_4$, a smaller particle size being a possible source for the different colors. Chemical analyses by ICP reveal that all compositions are shifted toward a higher SeO_4 content. These results have been confirmed by EDX analysis and from the evolution of the unit cell volume refined from XRPD data, see later (Table 1). From this table the following compositions can be deduced: $Cu_3(OH)_4(SO_4)_{0.6}(SeO_4)_{0.4}$, $Cu_3(OH)_4(SO_4)_{0.3}(SeO_4)_{0.7}$, and $Cu_3(OH)_4(SO_4)_{0.1}(SeO_4)_{0.9}$.

Physical Characterization. The elemental composition of each sample was determined on compressed pellets by an X-ray dispersive energy analyzer integrated to a JEOL 6700F scanning electron microscope (SEM), operating at an acceleration voltage of 18 kV. Thermal analysis was performed using a TA-SDT-Q600 apparatus operating at a 5 °C/min heating rate in a flow of air. Infrared spectra were recorded on an ATI Mattson spectrometer by transmission through KBr pellets containing ca. 1 mg of the compounds homogeneously dispersed. X-ray powder diffraction patterns were recorded at room temperature by means of a D5000 Siemens diffractometer (Cu $K\alpha_1$, 1.5406 Å).

The neutron diffraction experiments were performed at the Laboratoire Léon Brillouin (CEA Saclay) using the 3T2 and G4.1 diffractometers. Data obtained on the high-resolution powder diffractometer 3T2 ($\lambda = 1.2252$ Å, $6° < 2\theta < 126°$) were used for refinement of the nuclear structure at 300 K, and those from the multidetector (800 cells) G4.1 ($\lambda = 2.4266$ Å) were used for determination of the magnetic structure and its evolution as a function of temperature. Twelve diffraction patterns were recorded in the 2θ range 6°−85.9° at different temperatures between 1.4 and 15 K. The powder samples were set in a cylindrical vanadium container and held in an orange liquid helium cryostat. Nuclear and magnetic structures were refined using the FULLPROF program.[23] The nuclear scattering lengths ($b_{Cu} = 0.7718 \times 10^{-12}$ cm, $b_S = 0.2847 \times 10^{-12}$ cm, $b_{Se} = 0.7970 \times 10^{-12}$ cm, $b_O = 0.5803 \times 10^{-12}$ cm, $b_D = 0.6671 \times 10^{-12}$ cm, and $b_H = -0.3739 \times 10^{-12}$ cm) and copper (Cu^{2+}) magnetic form factor were those included in this program.

Magnetization (dc) measurements were performed in the range 2−300 K and from −50 to +50 kOe by means of a Quantum Design MPMS-XL SQUID magnetometer. ac susceptibilities in zero dc field were measured in the same apparatus using an ac field of 3.5 Oe oscillating at 15 Hz. Samples were placed in gelatin capsules and held in clear drinking straws.

Specific heat measurements were carried out using home-built equipment employing a quasi-adiabatic method in the range 1.6−35 K. The samples were ca. 200 mg pressed pellets wrapped in aluminum foil and thermally contacted with Apiezon grease. The final absolute heat capacity was extracted by subtraction of the contribution of the foil and the grease.

(19) (a) Boehm, M.; Roessli, B.; Schefer, J.; Wills, A. S.; Ouladdiaf, B.; Lelièvre-Berna, E.; Staub, U.; Petrakovskii, G. A. *Phys. Rev. B* **2003**, *68*, 024405-1-9. (b) Udod, L. V.; Sablina, K. A.; Pankrats, A. I.; Vorotynov, A. M.; Velikanov, D. A.; Petrakovskii, G. A.; Bovina, A. F. *Inorg. Mater.* **2003**, *39*, 1172−1180. (c) Petrakovskii, G.; Popov, M.; Martynov, S.; Roessli, B.; Schefer, J.; Ouladdiaf, B.; Boehm, M.; Staub, U.; Amato, A. *J. Magn. Magn. Mater.* **2004**, *272*−*276*, 199−200.

(20) Glaum, R.; Reehuis, M.; Stüsser, N.; Kaiser, U.; Reinauer, F. *J. Solid State Chem.* **1996**, *126*, 15−21.

(21) Nakua, A. M.; Greedan, J. E. *J. Solid State Chem.* **1995**, *118*, 402−411.

(22) Przenioslo, R.; Palewicz, A.; Regulski, M.; Sosnowska, I.; Ibberson, R. M.; Knight, K. S. *J. Phys: Condens. Matter.* **2006**, *18*, 2069−2075.

(23) Rodriguez-Carvajal, J. *FULLPROF: Rietveld, profile matching and integrated intensity refinement of X-ray and/or neutron data*, 3.5d version; Léon-Brillouin Laboratory: CEA Saclay, France, 1998.

Results and Discussion

Synthesis. $Cu_3(OH)_4SeO_4$ was obtained as a green powder under the conditions used in this work. Using a different procedure, Giester obtained it as dark green single crystals.[24] His procedure involved hydrothermal treatment of copper oxide rods, sodium carbonate $Na_2CO_3{\cdot}10H_2O$, and selenic acid H_2SeO_4 in the presence of a small quantity of water at 227 °C for 1 week. However, under such conditions a mixture of several phases was obtained, among them are $NaCu_2(OH)(H_2O)(SeO_4)_2$ and $Cu_3(OH)_4SeO_4$. The fact that different phases were obtained stimulates the search for another route to obtain a pure phase, particularly in view of studying the magnetic properties and neutron powder diffraction. The corresponding X-ray diffraction patterns of our samples confirm the presence of a unique phase according to JCPDF file No. 80-2494. In contrast, hydrothermal synthesis of $Cu_3(OH)_4SO_4$ resulted in single crystals at a lower temperature of 170 °C for a longer period of 6 days. However, the syntheses of the sulfate−selenate solid solution compounds only resulted in light green powders.

X-ray Powder Diffraction. The XRPD data of the samples $Cu_3(OH)_4(SO_4)_x(SeO_4)_{1-x}$, $x = 1$, 0.6, 0.3, 0.09, 0, recorded in the same conditions, clearly reveal that they are all related to the same crystalline structure,[24] the x variation inducing the expected line shift toward smaller Bragg angles with decreasing x. However, a strong dependence of the peak heights and peak widths of the Bragg reflections is observed, where the peak heights decrease while the peak widths increase with increasing selenate content. In contrast, the Bragg reflections for the pure selenate sample remain as sharp as those of the pure sulfate (Figure S1, Supporting Information). The unit cell and profile parameters have been refined using the Fullprof program in pattern matching mode (Table S1, Supporting Information). Assuming that the unit cell parameters vary according to Vegard's law,[25] it was therefore possible to determine the x content from the line joining the data of the samples $x = 1$ to 0 (Figure S2). Using the unit cell volume, the compositions given in Table 1 have been obtained, and they agree with the values deduced from EDX and ICP analyses. For the solid solutions, the particle sizes have been estimated using the Scherrer formula[26]

$$L = K\lambda/\beta(2\theta)\cos(\theta)$$

where L (in Å) is the size of the diffraction domain in the line direction, K is a constant (usually 0.9 for inorganic solids), λ is the wavelength of the X-ray beam (in Å), $\beta(2\theta) = (\beta^2_{exp} - \beta^2_{inst})^{1/2}$ is the line broadening calculated from the values of the full width at half-maximum (fwhm) for the sample, β_{exp}, and for the instrumental value, β_{inst}, $\cos(\theta)$ being the cosines of the diffraction angle (θ) for a line. In our case, the instrumental fwhm β_{inst} corresponds to the data measured for the pure sulfate, similar data being obtained for the pure selenate. In most cases, the particle sizes decrease linearly with decreasing x with mean values (from measurements on 10 diffraction lines) of 97, 55, and 36 nm for $x =$ 0.6, 0.3, and 0.09, respectively. The estimated values of the particle sizes, below 100 nm, confirm the previous hypothesis of its relation with the color of the samples.

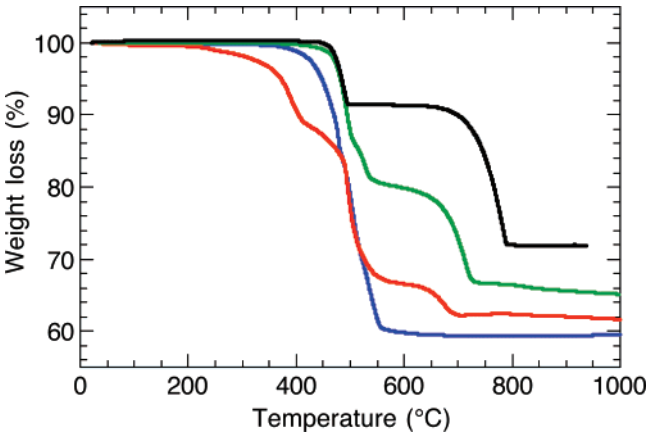

Figure 1. TGA traces recorded for $Cu_3(OH)_4SeO_4$ (blue line), $Cu_3(OH)_4(SeO_4)_{0.7}(SO_4)_{0.3}$ (red line), $Cu_3(OH)_4(SeO_4)_{0.4}(SO_4)_{0.6}$ (green line), and $Cu_3(OH)_4SO_4$ (black line) under air at a 5 °C/min heating rate.

Thermal Analysis. TGA of $Cu_3(OH)_4SeO_4$ (Figures 1 and S3) reveals a weight loss (obs = 40.6 wt %, calcd = 40.58 wt %) taking place in an almost continuous step between 420 and 560 °C. However, careful observations reveal the presence of two steps, associated with two peaks on the corresponding heat-flow curve centered at 460 and 505 °C. One expects decomposition in two steps: first OH groups as H_2O and second SeO_4 groups as SeO_3. For $Cu_3(OH)_4SeO_4$ the two steps are close to one another. In the case of $Cu_3(OH)_4SO_4$ the two steps are centered at 475 and 760 °C. The TGA traces recorded in the same conditions for the $Cu_3(OH)_4(SO_4)_x(SeO_4)_{1-x}$ samples reveal three-step weight loss for $x = 0.60$ and 0.30, each step being related to OH departure as H_2O, to selenate and sulfate decompositions as SeO_3 and SO_3. For $x = 0.09$, only two steps are visible. Increasing the selenate content in the solid solutions promotes a lower stability, the DTA effects being shifted to lower temperatures (Table S2).

Infrared Spectroscopy. Comparison of the infrared spectra of $Cu_3(OH)_4SeO_4$, $Cu_3(OD)_4SeO_4$, the corresponding sulfates, and the solid solutions $Cu_3(OH)_4(SO_4)_x(SeO_4)_{1-x}$ allows one to distinguish between the vibration bands related to XO_4 (X = S, Se) and OH(D) groups. While those of the first group appear at the same wavenumbers for H and D samples, those of the second group are shifted by a factor of 0.74, close to the expected value of $(18/17 \times 2)^{1/2}$. At low energy, i.e., below 500 cm^{-1}, the observed vibration bands are related to the Cu−O cores (Table S3, Figure S4). Concerning $Cu_3(OH)_4SeO_4$ and $Cu_3(OD)_4SeO_4$, the vibration bands of the SeO_4 group are expected at 833 (ν_1), 875 (ν_3), and 432 (ν_4) cm^{-1} for the isolated SeO_4 tetrahedron.[27] ν_3 appears as a triplet, 905, 884, and 843 cm^{-1}, in relation to the distorted local symmetry of the tetrahedron. For the same reason, the ν_1 vibration band (817 and 795 cm^{-1}), expected

(24) Giester, G.; *Monatsh. Chemie* **1991**, *122*, 229−234.
(25) Vegard, L.; Schjelderup, H. *Phys. Z.* **1917**, *18*, 93−96.
(26) Scherrer, P. *Göttinger Nachrichten* **1918**, *2*, 98.
(27) Nakamoto, K. *Infrared and Raman Spectra of Inorganic and Coordination Compounds*; John Wiley: New York, 1986.

Table 2. Crystallographic Data and Refinement Characteristics (Nuclear Cell) from Neutron Powder Diffraction Data Recorded at 300 K for $Cu_3(OD)_4XO_4$, X = Se, S

	$Cu_3(OD)_4SeO_4$	$Cu_3(OD)_4SO_4$
cryst syst	orthorhombic	
space group	*Pnma* (62)	
a (Å)	8.3844(2)	8.2574(2)
b (Å)	6.08405(9)	6.0529(1)
c (Å)	12.2829(2)	12.0099(2)
wavelength (Å)	1.2252	1.2252
2θ range (step)	6−125.7° (0.05)	6−125.7° (0.05)
reflns used/total	1087/1168	689/1033
no. of params	71	58
R_p (%)	10.3	6.72
R_{wp} (%)	10.5	6.32
R_{exp} (%)	4.93	4.48
R_B (%)	6.94	2.87
R_F (%)	3.85	1.99
GoF (%)	4.53	1.99

to be IR inactive in T_d symmetry, becomes active. The ν_4 is split, 447 and 400 cm^{-1}. The data are very similar for the D sample. For the solid solutions $Cu_3(OH)_4(SO_4)_x(SeO_4)_{1-x}$ one also observes the corresponding vibrations of the sulfate group that are at higher wavenumbers compared to the corresponding SeO_4 group with values of 1153, 1109, and 1070 cm^{-1} for ν_3, 987 cm^{-1} for ν_1, and 634, 613, and 602 cm^{-1} for ν_4 reported for pure sulfate.[27] No significant evolution of the positions of the $\nu(SO_4$ and $SeO_4)$ lines is observed for the solid solutions. Apart from the OH(D) stretching vibrations around 3500 (2500) cm^{-1}, some other lines are shifted when D substitutes for H (Table S3). They could be attributed to either OH(D) librations or ρ_R vibration modes.

Description of the Structure. Since the crystal structure of the selenate is isostructural to the sulfate and has been determined previously on a single crystal,[24,28] we will keep the discussion of our analysis brief and only highlight the key features to help with the discussion of the magnetic structure that will follow. The room-temperature neutron powder pattern of $Cu_3(OD)_4SeO_4$ has been used to refine the structure starting from the atomic coordinates obtained from the X-ray single crystal by Giester.[24] Table 2 gives the details of the refinement, Table 3 lists the final atomic positions, and Table S4 lists the interatomic bond lengths and angles. Figure S5 shows the observed and calculated profiles of the powder neutron diffraction pattern. The structure of $Cu_3(OD)_4SeO_4$ (Figure 2) can be described as three-legged ribbons of copper octahedra joined by μ_3-OH bridges and running along the *b* axis. These ribbons are further connected to each other by SeO_4 tetrahedra. The SeO_4 tetrahedra are nearly regular with a mean Se−O distance of 1.650 Å, the corresponding S−O distance in antlerite being 1.481 Å. This difference imposes certain constraints on the geometries of the two independent copper centers. The CuO_6 octahedra (Figure 3) are elongated according to the Jahn−Teller effect and edge-shared to form the three-legged ribbons. Cu(1) has four equatorial hydroxide, one axial hydroxide, and one axial selenate oxygen. We note that the deviation is as much as 10° within the equatorial plane and

(28) Hawthorne, F. C.; Groat, L. A.; Eby, R. K. *Can. Mineral.* **1989**, *27*, 205−209.

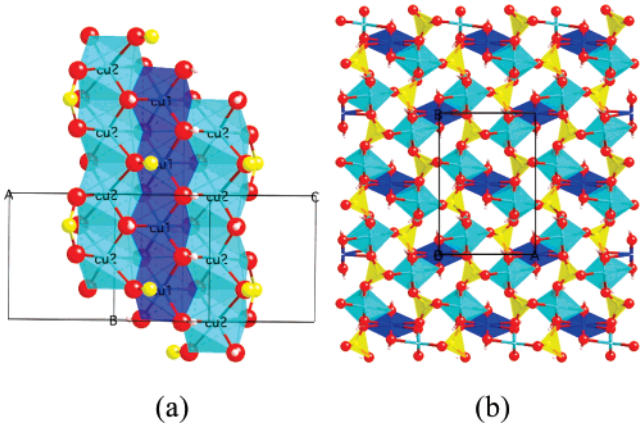

Figure 2. Crystal structure of $Cu_3(OD)_4SeO_4$: (a) a portion of the 3-legged brucite ribbon forming the skeleton of the structure showing the chains consisting of different Cu, and (b) projection of the structure along the ribbon showing the connections of the ribbons by the selenate in forming the 3D network.

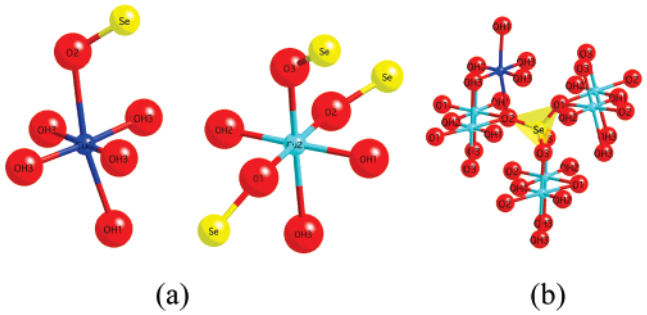

Figure 3. (a) Coordination of the crystallographically independent copper atoms, and (b) the first sphere of copper atoms around the selenate tetrahedron.

Table 3. Atomic Coordinates and Isotropic Thermal Motion Values at 300 K from Neutron Powder Data of $Cu_3(OD)_4SeO_4$[a]

atom	*x*/*a*	*y*/*b*	*z*/*c*	occupancy	*B* (Å^2)
Cu1	0.0037(7)	0.25	0.0016(3)	4.0	1.04(6)
Cu2	0.2814(3)	0.0011(4)	0.1284(2)	8.0	0.70(4)
Se	0.1294(4)	0.25	0.3655(3)	4.0	0.60(6)
O1	0.2702(6)	0.25	0.2710(4)	4.0	0.84(9)
O2	0.2111(7)	0.25	0.4867(4)	4.0	1.06(10)
O3	0.0243(3)	0.0225(5)	0.3490(2)	8.0	1.10(6)
OH1	0.2795(6)	0.25	0.0291(4)	4.0	0.54(8)
OH2	0.7175(6)	0.25	0.7793(4)	4.0	0.66(8)
OH3	0.0369(3)	0.5084(5)	0.1016(2)	8.0	0.64(5)
H1	0.3529(8)	0.25	0.9700(5)	0.44(4)	1.9(1)
D1	0.3529(8)	0.25	0.9700(5)	3.56(4)	1.9(1)
H2	0.1911(6)	0.75	0.2680(4)	0.30(4)	1.6(1)
D2	0.1911(6)	0.75	0.2680(4)	3.70(4)	1.6(1)
H3	0.5178(4)	0.0106(6)	0.6691(3)	0.40(5)	1.65(7)
D3	0.5178(4)	0.0106(6)	0.6691(3)	7.60(5)	1.65(7)

[a] D/(H + D) = 93%.

even larger (15°) between equatorial and axial oxygen atoms. Cu(2) has its elongated axis along O(1)−Cu(2)−O(2) where the two oxygen atoms are from two selenates. The equatorial plane is occupied by three hydroxide and one selenate oxygen atom. Cu(2) is less distorted with a maximum deviation of 7°. Comparison of these distances and angles to those of $Cu_3(OD)_4SO_4$ is given in Table S5. Whereas the four short Cu−O bonds are very similar for the S and Se equivalents, the two apical bonds are longer for the S sample. The oxygen atoms are of three types according to the number of bonds they involve with copper and selenium atoms. O3 and OD1

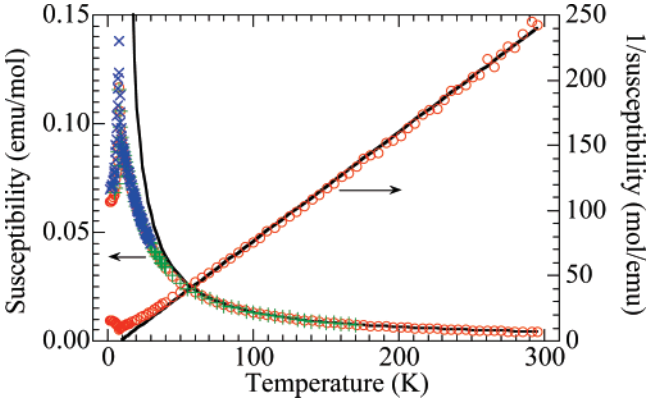

Figure 4. Temperature dependence of the ac (3.5 Oe, green plus) and dc susceptibilities of $Cu_3(OH)_4SeO_4$ measured in different applied fields (100 Oe, red circles; 0.65 Oe, blue crosses) and of the inverse dc susceptibility (red circles) in 100 Oe. The solid lines are the best fit of the data above 100 K to the Curie−Weiss law.

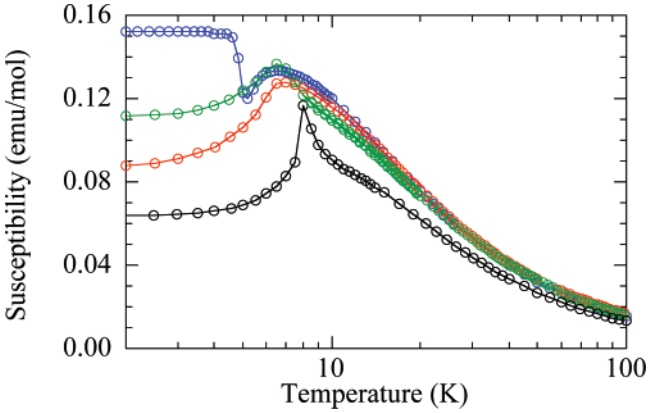

Figure 5. Semilog presentation of the temperature dependence of the dc susceptibilities measured in 100 Oe for $Cu_3(OH)_4SeO_4$ (black), $Cu_3(OH)_4(SO_4)_{0.3}(SeO_4)_{0.7}$ (green), $Cu_3(OH)_4(SO_4)_{0.6}(SeO_4)_{0.4}$ (red), and $Cu_3(OH)_4SO_4$ (blue).

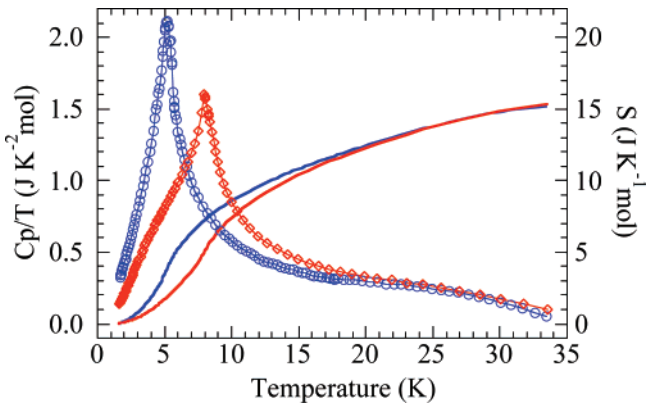

Figure 6. Temperature dependence of the zero-field temperature-normalized heat capacity of $Cu_3(OH)_4SeO_4$ (red) and $Cu_3(OH)_4SO_4$ (blue) and of the corresponding entropies (lines).

are μ_2-oxo and μ_2-hydroxo, respectively, O1, OD1, and OD3 are μ_3-oxo and μ_3-hydroxo, and O2 is μ_4-oxo. The O−D bond lengths (Table S6) are very close to each other with a mean value around 0.95 Å. All hydrogen bonds are weak and bifurcated, with O−D···O angles close to 140°. The X-ray powder diffraction data of the solid solutions are also identical to those of the two parent compounds, and their unit-cell parameters have been refined using pattern matching (Table S1). Of further importance in these structures, in relation to the magnetic properties, is the connectivity of the selenate to the copper atoms. Each selenate connects seven copper atoms belonging to three independent ribbons.

Magnetic Properties. The magnetic susceptibility (Figure 4) of $Cu_3(OD)_4SeO_4$ recorded under an applied field of 100 Oe follows above 100 K a Curie−Weiss law $\chi = C/(T - \theta)$ with $C = 1.166(9)$ emu K per mol and $\theta = +14(2)$ K. The Curie and Weiss constants were obtained by fitting the $1/\chi$ experimental data in the temperature range 100−300 K. The positive θ value indicates that the dominant nearest-neighbor exchange interaction within the ribbons is ferromagnetic. This conclusion is also supported by the continuous increase of the χT product between RT and ca. 50 K. From the Curie constant, $C = Ng^2\mu_B^2 s(s + 1)/3k$, of 0.389 emu K per Cu and $s = 1/2$ we deduced a value of the Landé g factor of 2.036. The effective moment $\sqrt{(8C)}$ of 1.763 μ_B is close to the expected value of 1.732, calculated with the spin-only formula.[29] At low temperature the magnetic susceptibility reaches a sharp maximum at 8 K (Figure 4) before decreasing at lower temperature. This behavior has been attributed to the presence of 3D antiferromagnetic ordering below the Néel temperature of 8 K. The presence of a peak at 8 K in the temperature dependence of only the real part of ac susceptibility and the lack of an imaginary component is consistent with antiferromagnetism having compensated moments. To confirm the latter, we measured the susceptibility in a very low field of 0.65 Oe and demonstrated that there is no spontaneous magnetization such as those for $Cu_3(OD)_4SO_4$.

In addition to the previously reported magnetic susceptibility of $Cu_3(OD)_4SO_4$ measured in 100 Oe, we re-measured the temperature dependence of its magnetization in different applied fields (1.2, 25, 100, and 500 Oe) to demonstrate the behavior of a classical canted-antiferromagnet (Figure S6). The magnetic susceptibilities of the solid solutions (Figure 5) were measured in 100 Oe field, and analysis of these data give $C = 1.457(7)$ emu K/mol ($x = 1$), 1.396(2) emu K/mol ($x = 0.6$), 1.302(2) emu K/mol ($x = 0.3$), and 1.170(5) emu K/mol ($x = 0.09$) and $\theta = +4.5(3)$ K ($x = 1$), +0.9(3) K ($x = 0.6$), +3.2(3) K ($x = 0.3$), and +13.1(8) K ($x = 0.09$). The low-temperature behavior of these compounds lies in between those of the two end members. In addition, there is no indication of spontaneous magnetization for all compositions.

Heat Capacity. The temperature dependence of the heat capacity of $Cu_3(OH)_4SeO_4$ shows a characteristic λ-type anomaly at $T = 8$ K indicating a phase transition toward a 3D state. Using the measured data, the magnetic component (C_m) is extracted by subtracting an AT^3 term representing the lattice contribution (Figure 6). It is compared to that of $Cu_3(OH)_4SO_4$. The entropy, estimated by integrating C_m/T versus T up to 35 K, is 15.2(1) J/K mol for the two compounds. This is in good agreement to the expected $3R$ $\ln(2s + 1)$. It is to be noted that a large fraction of this

(29) (a) Blundell, S. J. *Magnetism in Condensed Matter*; Oxford University Press: New York, 2001.
(30) *Supercell, a program to index superstructure reflections from a powder diffraction pattern*; Rodriguez-Carvajal, LLB. 1998.

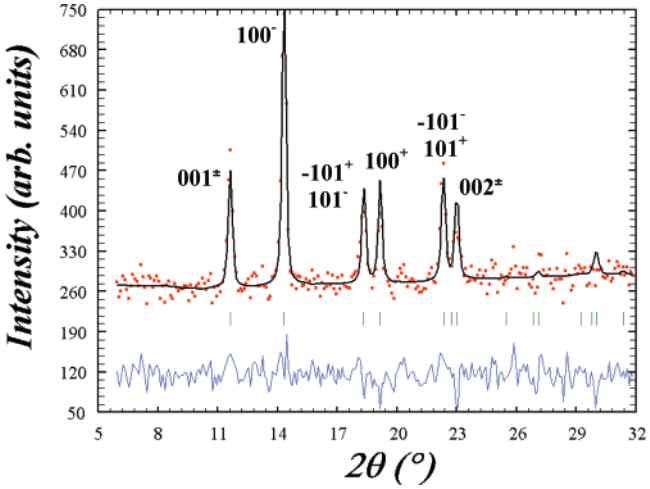

Figure 7. Observed (dotted line) and calculated (solid line) profiles of the difference plot from data recorded at 1.4 and 15 K on the G4.1 diffractometer, position of the magnetic reflections, and difference between observed and calculated profiles. The magnetic lines are indexed.

entropy is above the Néel transitions in relation to the low dimensional nature of the structures. It is, however, important to point out that observation of the full entropy means there is no geometrical frustration in the pseudo-triangular network of the magnetic moments within the ribbons.[31]

Magnetic Structure. Comparison of the neutron powder diffractograms recorded above and below T_N evidences the presence of new diffraction lines for the second one, suggesting antiferromagnetism. Moreover, one observes a shift of the position of these lines when the temperature increases from 3 to 7.5 K (Figures S7 and S8). Such a result is characteristic of the presence of an incommensurate magnetic structure. Using the Supercell program the magnetic propagation vector is found to be (0.1441, 0, 0) at 1.4 K,[30] i.e., a value very close to 1/7 along the *x* axis. The magnetic lines are not so intense due to the low moment of Cu (s = 1/2), and thus, the magnetic structure has been solved using the difference data between 1.4 and 15 K (Figure 7).

A noncollinear cycloidal structure with a propagation vector (1/7, 0, 0) fits best to the experimental data. The best refinement with R_{mag} = 12.7% yields a reasonable value of the magnetic moment as well as for the standard deviations of the different parameters (Table S7, Figure S9). The model consisting of antiparallel alignment of moments of ferromagnetic chains is in agreement with the results of the magnetic measurements that indicate the presence of short-range ferromagnetic interactions at high temperatures and a 3D antiferromagnetic order below the transition. However, the moment of Cu(1) remains random. Moreover, the magnetic structure is closely related to the one observed for the corresponding sulfate $Cu_3(OH)_4SO_4$. For the latter, the magnetic structure is commensurate with the magnetic

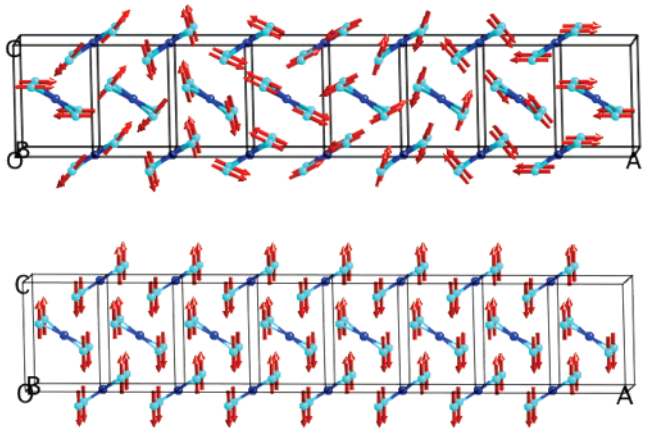

Figure 8. Magnetic structures of $Cu_3(OH)_4SeO_4$ (top) and $Cu_3(OH)_4SO_4$ (bottom) at 1.5 K showing the cycloidal commensurate k = 1/7 0 0 for the former and the collinear k = 0 0 0 AF order for the latter.

moments of the Cu2 atoms aligned along the *c* axis and no magnetic order along the central chain of Cu1 atoms. The same model is evidenced in the present case for all temperatures between 1.4 and 7.5 K with a decrease of the refined propagation vector component k_x from 0.1435(7) to 0.1110(16) and a slight decrease of the Cu2 magnetic moment (Figures 8, Table S8). It is important to note that the incommensurate magnetic structure above 3 K locks in to a commensurate one at 3 K, where the propagation vector is 1/7. The top panel of Figure 8 shows a projection of the magnetic moments of the copper atoms in $Cu_3(OH)_4SeO_4$ in the ac plane for adjacent unit cells in the *a*-axis direction to demonstrate the commensurate magnetic superstructure below 3 K. The bottom panel of Figure 8 is the equivalent view for $Cu_3(OH)_4SO_4$ where only a commensurate structure is observed. For each triple chain the magnetic moments of the copper ions (M = 0.88(5) μ_B at 1.4 K) belonging to the outer chains are oriented inside the ac plane, with ferromagnetic order inside a chain and antiferromagnetic order between the two outer chains of a ribbon. From one unit cell to the next along the *a* axis the magnetic moments make an angle of 51.5° and the corresponding rotation takes place in opposite directions for two outer chains belonging to the same three-legged ribbon. In such a way, the AF ordering is kept through the rotation. Using $M = M_s(1 - T/T_N)^\beta$ to fit the temperature dependence of the moment, as shown in Figure 9, in order to extract the critical exponent gave M_s = 0.90(1) μ_B, T_N = 7.82(9) K, and β = 0.111(2). The latter indicates that the material is behaving as a 2d-Ising where β = 1/8.[32]

There are two important facets of the magnetic properties and magnetic structures that would be interesting to find a rationale for the different behaviors between the two compounds. One is the observation of an idle moment for Cu(1), the copper atom in the middle leg of the ribbon, and the other is the complexity in the magnetic structures, that is a cycloidal versus a collinear ordering.

Concerning the idle moment of Cu(1), which means a random orientation of the moments in the crystals, it may

(31) (a) Bramwell, S. T.; Gingras, M. J. P. *Science* **2001**, *94*, 1495. (b) Greedan, J. E. *J. Mater. Chem.* **2001**, *11*, 37. (c) Ramirez, A. P. In *Handbook of Magnetic Materials*; Buschow, K. J. H., Ed.; Elsevier Science: Amsterdam, 2001; Vol. 13, p 423. (d) Grohol, D.; Matan, K.; Cho, J.-H.; Lee, S.-H.; Lynn, J. W.; Nocera, D. G.; Lee, Y. S. *Nat. Mater.* **2005**, *4*, 323. (e) *Magnetic Systems with Competing Interactions: Frustrated Spin Systems*; Diep, H. T., Ed.; World Scientific: Singapore, 1994.

(32) Stanley, H. E. *Introduction to Phase Transitions and Critical Phenomena*; Clarendon Press: Oxford, 1971; p 47.

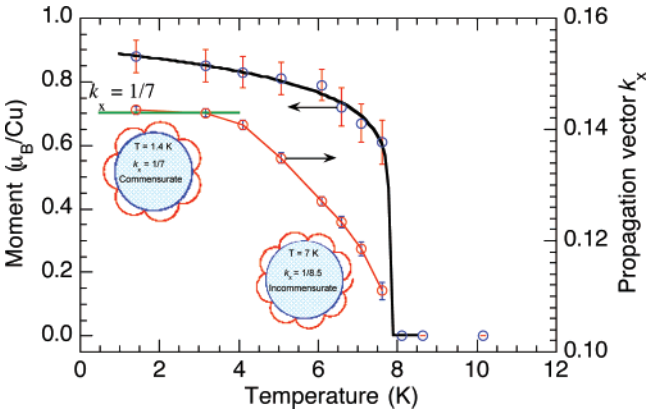

Figure 9. Temperature dependence of the magnetic moment (blue circles) and propagation vector (red circles) for $Cu_3(OH)_4SeO_4$. The solid black line is the 2d-Ising model fit, and the green line marks the commensurate $k = 1/7\ 0\ 0$. The red line is a guide to the eye. The commensurabilities are demonstrated by the Huygens' figures where the red semicircles represent the nuclear lattice and the blue circles the magnetic lattice periodicity.

be random within a chain or ordered within a chain but random between chains. The fact that the estimated entropies from the heat capacity measurements for both compounds are those expected for three ordered moment ($S = 1/2$) would suggest that there is ordering within a chain but randomness between chains. Furthermore, the observed entropies and the fact that the ratios of the Weiss constant to the Néel temperature are less than five would eliminate any possibility of frustration within the pseudo-triangular organized copper moments in the ribbons. Another point is that for the three moments per formula unit one may anticipate a ferrimagnetic ground state. This is certainly not the case for the two compounds. As such one may also propose that the moments of Cu(1) of one chain must compensate for those of the neighboring ones to result in a compensated Néel state. If one now considers the coupling between the outer copper atoms (Cu2) of the ribbon with those of neighboring ribbons there are five neighboring equivalent copper from different ribbons with which super-super-exchange via the sulfate groups must be taken into consideration.

Concerning the difference in magnetic structures, consideration of the distances and angles may provide some clues to the effect. In Table S5 we listed the major differences. Although there are quite large differences of up to 0.1 Å and 4.9° the angles are not borderline for transforming the exchange from antiferromagnetic to ferromagnetic if we assume a critical angle of 98° for Cu−O−Cu. DFT calculations will be required to rationalize the observations.

Conclusion

A rare occurrence of a cycloidal magnetic structure, commensurate ($k = 1/7,0,0$) with the nuclear lattice for $T \leq 3$ K and incommensurate for $T > 3$ K, is observed for the antiferromagnet $Cu_3(OH)_4SeO_4$. In contrast, the canted antiferromagnet $Cu_3(OH)_4SO_4$ has a simple magnetic structure with $k = 0,0,0$. The neutron diffraction results suggest random ordering for the moments of the copper atoms in the middle chain of each ribbon for both compounds, while magnetic data and, in particular, heat capacity results suggests ordering within a chain but randomness between ribbons. Replacement of SO_4 by SeO_4 results in isostructural solid solutions and almost continuous magnetic and thermal behaviors lying between the two extremes.

Acknowledgment. We gratefully acknowledge the CNRS-France for funding.

Supporting Information Available: Infrared, DT-TGA, nuclear and magnetic crystallographic (tables of bond lengths and angles), and magnetic data for compounds **1** and **2**. This material is available free of charge via the Internet at http://pubs.acs.org.

IC700900B